Journal of
**Applied Crystallography**

ISSN 0021-8898

Received 14 January 2010
Accepted 30 April 2010

# Comparative study of two lead-free piezoceramics using diffraction techniques

**Ljubomira Ana Schmitt,[a]* Manuel Hinterstein,[b] Hans-Joachim Kleebe[a] and Hartmut Fuess[b]**

[a]Institute of Applied Geosciences, Darmstadt University of Technology, Darmstadt, D-64287, Germany, and [b]Institute of Materials Science, Darmstadt University of Technology, Darmstadt D-64287, Germany. Correspondence e-mail: ljuba@st.tu-darmstadt.de

A comparative study of two distinct lead-free piezoceramics, $(Bi_{0.5}Na_{0.5}TiO_3)_{0.92}$–$(BaTiO_3)_{0.06}$–$(K_{0.5}Na_{0.5}NbO_3)_{0.02}$ and $(Bi_{0.5}Na_{0.5}TiO_3)_{0.94}$–$(BaTiO_3)_{0.05}$–$(K_{0.5}Na_{0.5}NbO_3)_{0.01}$, termed 92-06-02 and 94-05-01, respectively, is presented. The samples were investigated by complementary diffraction techniques, namely X-ray, neutron and electron diffraction. Transmission electron microscopy (TEM) and powder diffraction experiments clearly revealed the presence of both rhombohedral and tetragonal phases in space groups *R*3*c* and *P*4*bm*, respectively. Superlattice reflections observed in the diffraction patterns were used to identify the two phases. It was found that sample 92-06-02, with a high proportion of the nonpolar tetragonal phase, shows a grainy contrast, whereas specimen 94-05-01 features domain-like contrast, related to a higher rhombohedral phase fraction. The combination of local scale analyses *via* TEM with X-ray and neutron diffraction provides the experimental basis for further structural investigations.



## 1. Introduction

For the past few decades, lead-containing ceramics have been the material of choice for actuator and sensor applications. With regard to environmental issues, research on lead-free compounds is of great technological importance (Saito *et al.*, 2004; Maeder *et al.*, 2004; Takenaka *et al.*, 2007; Zhang *et al.*, 2007; Rödel *et al.*, 2009). Because of their outstanding properties (Rödel *et al.*, 2009; Maeder *et al.*, 2004; Zhang, Kounga, Aulbach, Jo *et al.*, 2008), lead-free ceramics, containing $Bi_{0.5}Na_{0.5}TiO_3$ (BNT), $BaTiO_3$ (BT) and $K_{0.5}Na_{0.5}NbO_3$ (KNN), are of great interest as possible lead-free piezoelectric materials.

Structural studies of BNT were undertaken by Jones & Thomas (2002). In the temperature range 573–593 K, they detected two temperature-dependent phase transitions, from the low-temperature ferroelectric phase in space group *R*3*c* to the high-temperature phase in space group *P*4*bm*. They assigned the ferroelectric to paraelectric phase transition to 813 K (Jones & Thomas, 2002). Both polar ferroelectric phases exhibit octahedral tilting, which can be described by the Glazer (1975) notation as $a^-a^-a^-$ for the *R*3*c* phase and $a^0a^0c^+$ for the *P*4*bm* phase. The octahedral tilting results in superlattice reflections of the type 1/2{*ooo*} for *R*3*c* and 1/2{*ooe*} for *P*4*bm* (Woodward & Reaney, 2005; Kishida *et al.*, 2009), where *o* and *e* denote odd and even Miller indices, respectively. Dorcet & Trolliard (2008) observed these kinds of superstructure reflections in the BNT system using transmission electron microscopy (TEM). They described the existence of thin tetragonal platelets within a rhombohedral matrix. For the *P*4*bm* phase, Jones & Thomas (2000, 2002) reported an unusual combination of in-phase octahedral tilting and antiparallel cation displacements.

Preliminary electromechanical measurements revealed a giant strain of 0.45% at an electric field of 8 kV mm$^{-1}$ for the composition $(Bi_{0.5}Na_{0.5}TiO_3)_{0.92}$–$(BaTiO_3)_{0.06}$–$(K_{0.5}Na_{0.5}NbO_3)_{0.02}$, hereinafter abbreviated as 92-06-02 (Zhang *et al.*, 2007; Zhang, Kounga, Aulbach, Granzow *et al.*, 2008). This giant strain was attributed to a field-induced nonpolar to ferroelectric phase transition (Jo *et al.*, 2009). A grainy contrast was observed in TEM experiments for this composition reported in a previous study (Zhang, Kounga, Aulbach, Granzow *et al.*, 2008). The structure at room temperature was studied by X-ray diffraction (XRD) and TEM by Zhang and co-workers (Zhang *et al.*, 2007; Zhang, Kounga, Aulbach, Granzow *et al.*, 2008). Based on uni- and bipolar strain measurements, the analysed ceramics were categorized into two groups. Group I compositions have a dominant ferroelectric order, while group II compositions exhibit mixed ferroelectric and antiferroelectric order. The specific order was previously denoted as antiferroelectric (Zhang *et al.*, 2007), although more recently it has been labelled as nonpolar order (Jo *et al.*, 2009). Based on dielectric measurements, Zhang, Kounga, Aulbach, Granzow *et al.* (2008) assigned specimen 92-06-02 to group II and 94-05-01 to group I.

The developed domain configurations of sample 91-06-03 (Kling *et al.*, 2010) under an applied electric field were comparable with the initial morphology of sample 94-05-01

**Table 1**
Fractional atomic coordinates and equivalent isotropic displacement parameters (Å$^2$) from the refinements of samples 94-05-01 and 92-06-02.

| Atom | $x$ | $y$ | $z$ | $U_{iso}$ |
|---|---|---|---|---|
| 92-06-02, *P4bm* | | | | |
| *A* | 0.0 | 0.5 | 0.549 (4) | 0.0543 (18) |
| *B* | 0.0 | 0.0 | 0.0 | 0.0045 (15) |
| $O_1$ | 0.0 | 0.0 | 0.518 (6) | 0.0317 (6) |
| $O_{2,3}$ | 0.2393 (5) | 0.2607 (5) | 0.047 (3) | 0.0317 (6) |
| 94-05-01, *P4bm* | | | | |
| *A* | 0.0 | 0.5 | 0.561 (7) | 0.056 (4) |
| *B* | 0.0 | 0.0 | 0.0 | 0.015 (3) |
| $O_1$ | 0.0 | 0.0 | 0.520 (11) | 0.0384 (14) |
| $O_{2,3}$ | 0.2369 (6) | 0.2631 (6) | 0.053 (5) | 0.0384 (14) |
| 94-05-01, *R3c* | | | | |
| *A* | 0.0 | 0.0 | 0.2750 (8) | 0.033 (3) |
| *B* | 0.0 | 0.0 | 0.0102 (9) | 0.001 (2) |
| O | 0.1239 (14) | 0.333 (2) | 0.08333 | 0.0230 (13) |

(§3.2). However, until now no attempt had been made to combine several diffraction techniques, including studies on a local scale *via* TEM and bulk methods using XRD and neutron diffraction, for this lead-free material class. Hence, this work comprises a comparative study of compositions 92-06-02 and 94-05-01, using X-ray, neutron and electron diffraction.

## 2. Experimental

For this examination, ceramics with compositions 92-06-02 and 94-05-01 were chosen. Samples were produced by a conventional solid-state sintering method from $Bi_2O_3$, $Na_2CO_3$, $BaCO_3$, $TiO_2$, $K_2CO_3$, $Na_2CO_3$ and $Nb_2O_5$ powders, sintered at 1373 K. Further information on specimen synthesis is given elsewhere (Zhang *et al.*, 2007; Zhang, Kounga, Aulbach, Granzow *et al.*, 2008).

### 2.1. Powder diffraction

All high-resolution X-ray measurements were performed at the powder diffraction beamline B2 at HASYLAB (DESY, Hamburg, Germany) at an incident wavelength of $\lambda \simeq 0.5$ Å (25 keV) using transmission geometry. Data were recorded by an NaI scintillation counter in 0.004° steps. Neutron powder diffraction measurements were carried out on the SPODI powder diffractometer at the research reactor FRM-II (Garching, Germany) (Hoelzel *et al.*, 2007) at an incident wavelength of 1.548 Å. Data were collected by a bank of 80 position-sensitive $^3$He detectors, covering a 160° scattering range.

Full-profile Rietveld refinements were carried out using the software package *FULLPROF* (Roisnel & Rodriguez-Carvajal, 2001). The peak profile shape was described by a pseudo-Voigt function (Thompson *et al.*, 1987). The backgrounds of the diffraction patterns were fitted using linear interpolation between selected data points in non-overlapping regions. The scale factor, lattice parameters, atomic positions, isotropic displacement factors, zero angular shift and profile shape parameters were varied during the refinement. To combine information from X-ray and neutron diffraction, refinements were performed simultaneously with both data sets. Therefore, the atomic positions and the lattice parameters were constrained for X-ray and neutron data.

**Table 2**
Structural parameters.

| | *P4bm* | *R3c* |
|---|---|---|
| 92-06-02 | | |
| $a$ (Å) | 5.52097 (12) | – |
| $c$ (Å) | 3.90535 (16) | – |
| $a_c$ (Å) | 3.90392 | – |
| $\alpha, \beta, \gamma$ (°) | 90, 90, 90 | – |
| Volume (Å$^3$) | 119.039 (6) | – |
| Lattice distortion (%) | 0.036 (6) | – |
| $\omega$ (°) | 2.45 (12) | – |
| $P_s$ (μC cm$^{-2}$) | 3.4 (16) | – |
| Number of refined parameters | 43 | |
| $R_p$ | 0.0342 | |
| $R_{wp}$ | 0.0437 | |
| 94-05-01 | | |
| $a$ (Å) | 5.5194 (5) | 5.5014 (4) |
| $c$ (Å) | 3.9032 (5) | 13.5845 (12) |
| $a_c$ (Å) | 3.9028 | 3.9006 |
| $\alpha, \beta, \gamma$ (°) | 90, 90, 90 | 90, 90, 120 |
| $\alpha_r$ (°) | – | 89.69 |
| Volume (Å$^3$) | 118.91 (2) | 356.06 (5) |
| Lattice distortion (%) | 0.01 (2) | 0.81 (2) |
| $\omega$ (°) | 3.00 (15) | 8.49 (1) |
| $P_s$ (μC cm$^{-2}$) | 6.8 (37) | 33.2 (19) |
| Phase fraction | 0.60 (2) | 0.40 (2) |
| Number of refined parameters | 55 | |
| $R_p$ | 0.0879 | |
| $R_{wp}$ | 0.0813 | |

### 2.2. TEM

For TEM investigation, samples were prepared by a standard procedure of polishing, disc cutting, dimpling and ion milling. Thin slices were polished down to approximately 120 μm thickness, ultrasonically cut into discs of 3 mm diameter, mechanically dimpled and thinned on both sides by an $Ar^+$ ion beam. Specimens were lightly coated with a thin carbon coat to prevent charging under the incident electron beam. The experiments were carried out on a Philips CM20 Super twin microscope operating at 200 kV using a double tilt holder. The orientation matrices of the grains were directly determined by a program for interpreting electron diffraction patterns (*PIEP*; Miehe, 2002). Zone axes were indexed according to a cubic structure. Representative grains were examined on the $[011]_c$, $[111]_c$, $[013]_c$ and $[031]_c$ zone axes. The intensities of the superstructure reflections of the selected-area electron diffraction (SAED) patterns, of both compositions, were compared within different zone axes.

## 3. Results and discussion

The 1/2{*ooo*} and 1/2{*ooe*} superstructure reflections indicate the presence of $a^-a^-a^-$ and $a^0a^0c^+$ octahedral tilting (Glazer, 1975; Woodward & Reaney, 2005; Kishida *et al.*, 2009). These two superstructure reflections imply the existence of a

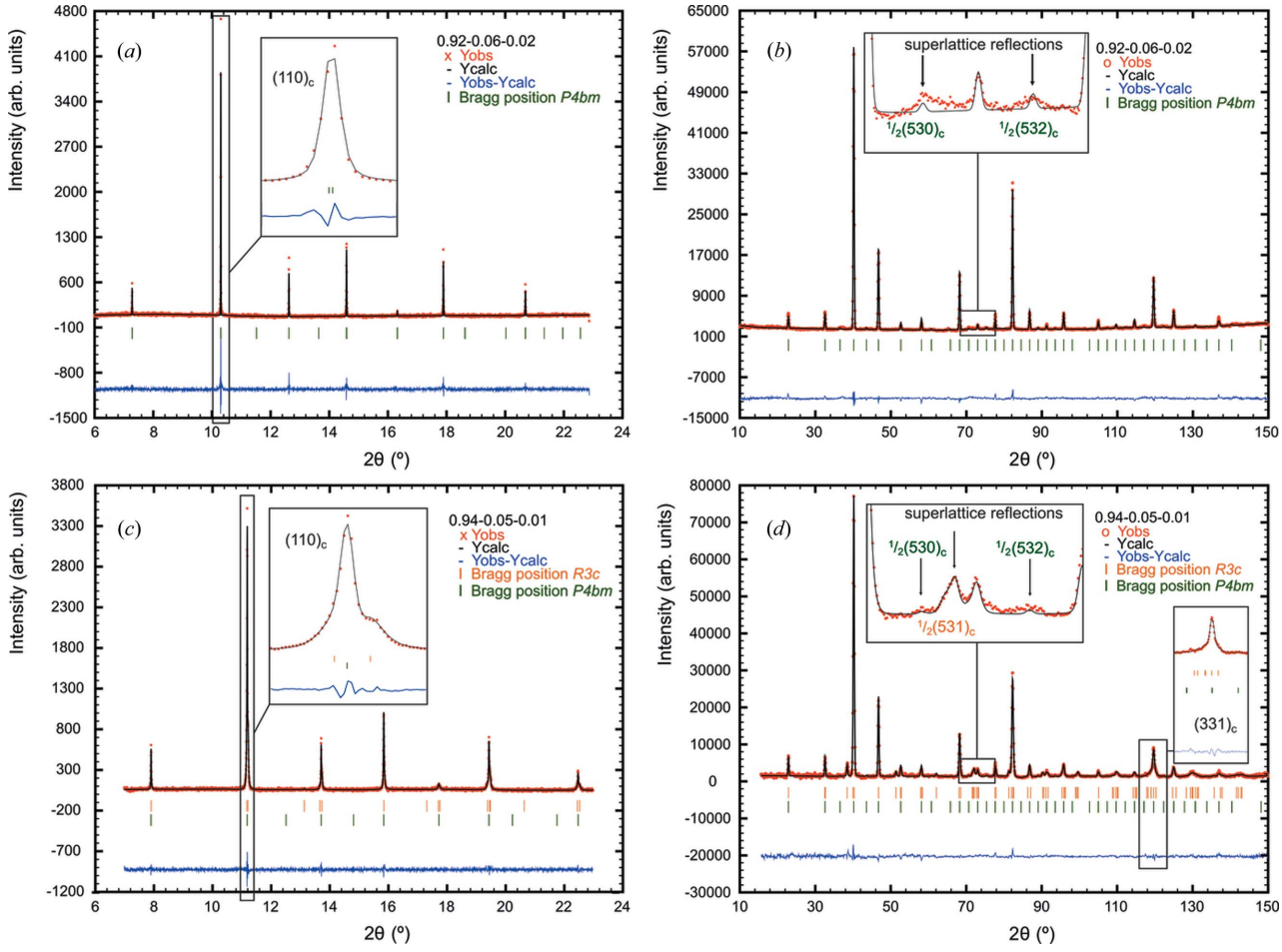


**Figure 1**
Rietveld refined X-ray and neutron diffraction data of (*a*), (*b*) sample 92-06-02 and (*c*), (*d*) sample 94-05-01. (*a*) The refinement of 92-06-02 from high-resolution X-ray data yields a weak ferroelectric distortion from cubic symmetry. (*b*) High-resolution neutron diffraction data show the 1/2{*ooe*} superlattice reflections, which are significantly broadened (inset). (*c*) X-ray diffraction data from specimen 94-05-01. The coexistence of tetragonal *P*4*bm* and rhombohedral *R*3*c* phases is visible. (*d*) Neutron diffraction data. Strong rhombohedral and weak tetragonal superstructure reflections are visible in the inset.

rhombohedral *R*3*c* and a tetragonal *P*4*bm* phase, respectively. Hence, the presence or absence of these two superstructure reflections enables a phase determination.

### 3.1. Powder diffraction

In Fig. 1, the combined Rietveld refinements from X-ray (Figs. 1*a* and 1*c*) and neutron diffraction data (Figs. 1*b* and 1*d*) are presented. The refinement of 92-06-02 yields a weak ferroelectric distortion from cubic symmetry (Fig. 1*a*). The *c*/*a* ratio is about 1.0004 and the atomic displacements show the same unusual antiparallel cation displacement, consistent with the observation of Jones & Thomas (2000) for $Bi_{0.5}Na_{0.5}TiO_3$ (Table 1). With high-resolution neutron diffraction we observed 1/2{*ooe*} superlattice reflections (Fig. 1*b*, inset), due to the existence of in-phase tilting of oxygen octahedra. This corresponds, according to Glazer notation, to the $a^0a^0c^+$ tilt system in the space group *P*4*bm*.

Atomic positions and lattice parameters were taken as the basis for calculating the octahedral tilting angle $\omega$ and the spontaneous polarization $P_s$ (Table 2). The estimation of $P_s$ is based on the dipole moment equation $P_s \simeq (1/V)\sum_i q_i r_i$, with the sum over all point charges $q_i$ at positions $r_i$ in a primitive cell volume $V$ (Frantti *et al.*, 2002). The Rietveld refinement of 92-06-02 revealed a low spontaneous polarization and a small octahedral tilting angle of $\omega_c = 2.45°$, which can only be observed with neutron diffraction. Compared with the pseudocubic reflections of the neutron and X-ray data, the tetragonal superlattice reflections are broadened significantly. We assign this to size broadening due to short-range order of the octahedral tilting, whereas the pseudocubic matrix exhibits long-range order.

Analysis of the X-ray diffraction data from the combined refinement of 94-05-01 is depicted in Fig. 1(*c*). The coexistence of the tetragonal *P*4*bm* and low-temperature rhombohedral *R*3*c* phases is visible. While the tetragonal phase exhibits nearly the same pseudocubic character as 92-06-02 ($c/a$ = 1.0001, $\omega_c = 3.0°$), the rhombohedral phase is significantly distorted (Table 2). The cell transformation from hexagonal to rhombohedral yields a rhombohedral distortion angle of 89.69°. In the neutron diffraction data the tetragonal 1/2{*ooe*} superlattice reflections are barely visible, compared with the

pronounced rhombohedral 1/2{*ooo*} superlattice reflections. Higher indexed reflections clearly show a two-phase coexistence (Fig. 1*d*, inset). The rhombohedral superlattice reflections originate from antiphase tilting of oxygen octahedra and are described by an $a^-a^-a^-$ tilt system for space group *R*3*c*. In contrast with the tetragonal tilt system, a pronounced tilt angle of $\omega_a = 8.49^\circ$ was observed by neutron diffraction for the rhombohedral $a^-a^-a^-$ tilt system, which is still not observable in the X-ray diffraction data (Fig. 1*c* and Table 2).

For 94-05-01, the atomic positions of the space group *P*4*bm* again exhibit an unusual combination of in-phase tilting and antiparallel cation shifts, as reported for BNT (Jones & Thomas, 2000, 2002) (Table 1). The spontaneous polarization of the tetragonal *P*4*bm* phase of 94-05-01 shows a similar low value to that of 92-06-02, while it is significantly higher for *R*3*c* (Table 2). These two phases, having such a pronounced difference in spontaneous polarization, indicate the coexistence of a nonpolar and a ferroelectrically active phase in 94-05-01.

### 3.2. TEM

In Fig. 2(*a*) a bright-field (BF) image of sample 92-06-02 is depicted. The grains show, consistent with previous TEM studies (Zhang, Kounga, Aulbach, Granzow *et al.*, 2008), an average grain size of about 1 µm. The major fraction of these show a grainy morphology, comparable to relaxor type ferroelectrics (Dai *et al.*, 1995*a*,*b*; Gupta *et al.*, 1998). Within the grains, areas of several hundred nanometres across are frequently observed, showing a lamellar domain-like contrast (marked by an arrow). Sample 94-05-01 (Fig. 2*b*), which is largely ferroelectric (Zhang, Kounga, Aulbach, Granzow *et al.*, 2008; Tan *et al.*, 2009), exhibits a grain morphology similar to the domains observed in $Pb(Zr_{1-x}Ti_x)O_3$ (PZT) ceramics (Cao & Randall, 1996; Woodward *et al.*, 2005; Schmitt *et al.*, 2007). For example, PZT specimens with compositions between $Pb(Zr_{0.55}Ti_{0.45})O_3$ and $Pb(Zr_{0.60}Ti_{0.40})O_3$, belonging to the rhombohedral side of the morphotropic phase boundary (MPB) and exhibiting a mixture of lamellar and irregular domains, closely resemble the domain morphology of 94-05-01 (Schmitt *et al.*, 2007). However, a few regions with lamellar domains comparable to $Pb(Zr_{0.45}Ti_{0.55})O_3$ were also observed.

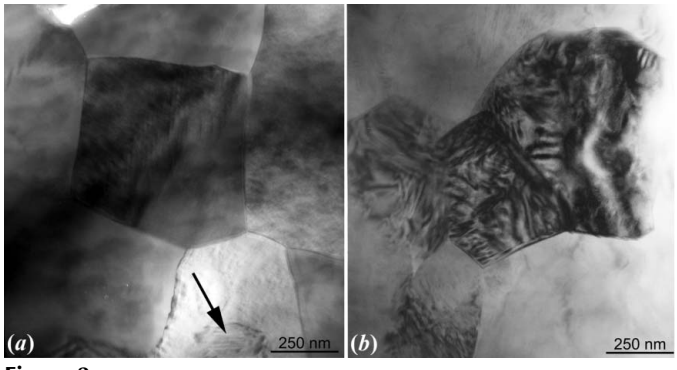


**Figure 2**
(*a*) TEM bright-field (BF) image of specimen 92-06-02. A grainy morphology is visible. Within the grains, areas of several hundred nanometres across, with a lamellar domain-like contrast, are frequently observed (marked by an arrow). (*b*) TEM BF image of sample 94-05-01, showing a high fraction of lamellar domain-like regions.

**Table 3**
Zone axes and corresponding observable superstructure reflections and phases.

T denotes tetragonal and R rhombohedral.

| $\langle$Zone$\rangle_c$ | Superstructure reflections | Phase |
|---|---|---|
| 001 | 1/2{*ooe*} | T |
| 101 | 1/2{*ooo*} | R |
| 111 | 1/2{*ooe*} | T |
| 102 | 1/2{*ooe*} | T |
| 112 | 1/2{*ooe*} and 1/2{*ooo*} | T and R |
| 212 | 1/2{*ooe*} | T |
| 103 | 1/2{*ooe*} and 1/2{*ooo*} | T and R |
| 113 | 1/2{*ooe*} | T |
| 203 | 1/2{*ooe*} | T |
| 213 | 1/2{*ooe*} and 1/2{*ooo*} | T and R |
| 223 | 1/2{*ooe*} | T |

SAED revealed no spot splitting but showed the 1/2{*ooo*} and 1/2{*ooe*} superstructure reflections, due to $a^-a^-a^-$ and $a^0a^0c^+$ octahedral tilting, which is consistent with our X-ray and neutron diffraction experiments. Based on thermodynamic theory, Rossetti & Khachaturyan (2007) showed that, towards the MPB, the domain wall energy decreases. The lattice distortion decreases (Schönau *et al.*, 2007), leading to the nanoscale domain structures observed for PZT ceramics (Schmitt *et al.*, 2007; Schönau *et al.*, 2007). In the lead-free 94-05-01 system this is even more pronounced. Concerning the small tetragonal *c*/*a* ratio of 1.0004 and rhombohedral angle of $\alpha = 89.69^\circ$ obtained from neutron diffraction data, a possible spot splitting cannot be resolved in the SAED pattern.

In Table 3, the zone axes and the corresponding superstructure reflections and phase are listed. In the $\langle 001\rangle_c$ and $\langle 111\rangle_c$ zone axes, the 1/2{*ooe*} superstructure reflections are visible. The 1/2{*ooo*} superstructure reflections are visible in the $\langle 110\rangle_c$ zone. Both types of superstructure reflections can be studied, for example, in the $\langle 112\rangle_c$, $\langle 103\rangle_c$, $\langle 213\rangle_c$ *etc.* zones. In Fig. 3, SAED patterns from specimen 92-06-02 (left column) and 94-05-01 (right column) are shown. Figs. 3(*a*) and 3(*b*) show the SAED patterns of the $[011]_c$ zone axis. Sample 92-06-02 shows weak 1/2{*ooo*} superlattice reflections (Fig. 3*a*), whereas specimen 94-05-01 shows strongly excited 1/2{*ooo*} superlattice reflections (Fig. 3*b*), revealing a higher proportion of the rhombohedral phase for sample 94-05-01, consistent with a previous study of 94-05-01 by Tan *et al.* (2009). In Figs. 3(*c*) and 3(*d*), SAED patterns along $[111]_c$ are depicted. The 1/2{*ooe*} superstructure reflections in Fig. 3(*c*) are strongly excited, whereas in Fig. 3(*d*) they are extremely weak, leading to the conclusion that the tetragonal phase fraction in sample 92-06-02 is significantly higher than in specimen 94-05-01. Zone axis $[013]_c$ shows both types of superlattice reflections and confirms the aforementioned observation ($[011]_c$ and $[111]_c$ zone). Sample 92-06-02 shows strong 1/2{*ooe*} and weak 1/2{*ooo*} superstructure reflections (Fig. 3*e*), while specimen

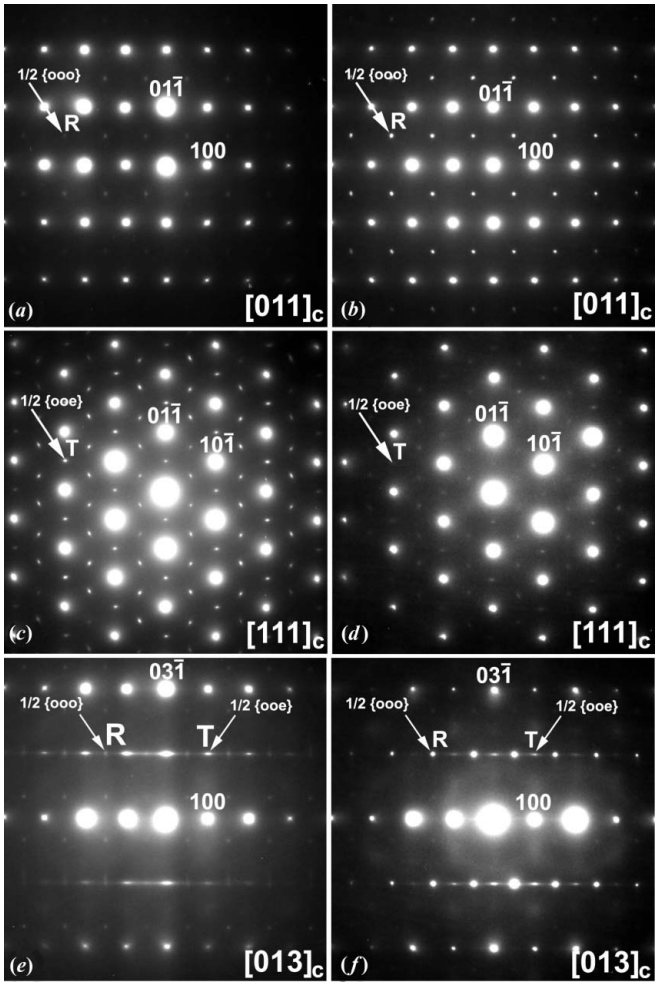


**Figure 3**
Selected-area electron diffraction (SAED) patterns of the $[011]_c$, $[111]_c$ and $[013]_c$ zone axes. Arrows indicate the 1/2{*ooo*} and 1/2{*ooe*} superstructure reflections, where R means rhombohedral and T tetragonal. The left-hand column shows the zone axis diffraction patterns for sample 92-06-02 and the right-hand column those for 94-05-01. (*a*) The weak intensity of the 1/2{*ooo*} superlattice reflections, due to a low proportion of the rhombohedral phase. (*b*) The bright intensity of the 1/2{*ooo*} superlattice reflections, implying a high proportion of the rhombohedral phase. (*c*) The bright intensity of the 1/2{*ooe*} superlattice reflections, due to a high fraction of the tetragonal phase. (*d*) The weak intensity of the 1/2{*ooe*} superstructure reflections, signifying a low fraction of the tetragonal phase. (*e*) In the $[013]_c$ zone both superstructure reflections are visible. The 1/2{*ooo*} are weaker than the 1/2{*ooe*} superlattice reflections. Streaking of the 1/2{*ooe*} superlattice reflections in the [100] direction is visible. (*f*) In contrast with Fig. 2(*e*), the 1/2{*ooo*} superstructure reflections are stronger than the 1/2{*ooe*}, which is consistent with observations along the $[011]_c$ and $[111]_c$ zone axes.

94-05-01 reveals strong 1/2{*ooo*} and weak 1/2{*ooe*} superlattice reflections.

The tetragonal superlattice reflections show streaking along the [100] direction. Tetragonal orientational variants, present as small platelets, lead to an elongation of the superlattice reflections, as described by Dorcet & Trolliard (2008). They predicted a nanostructured tetragonal phase within a rhombohedral matrix, but we assign the observed presence of both types of superstructure reflections to the coexistence of the rhombohedral *R*3*c* and tetragonal *P*4*bm* phases, which develop below the Curie temperature, although in different proportions depending on the composition. This was verified through an *in situ* hot-stage TEM experiment on sample 94-05-01 by Kling (2010). Both tetragonal 1/2{*ooe*} and rhombohedral 1/2{*ooo*} superlattice reflections were retained during heating below the Curie temperature, albeit with different intensities. Depending on the temperature, wide rhombohedral/tetragonal and tetragonal/cubic phase coexistence regions were also described by Jones & Thomas (2002) for BNT ceramics.

A detailed TEM study of 91-06-03, which comprised SAED and dark-field imaging, showed clear evidence for the coexistence of the rhombohedral *R*3*c* and tetragonal *P*4*bm* phases within single grains at room temperature (Schmitt & Kleebe, 2010). A distinct correlation was observed between the superstructure reflections of the SAED pattern and the excited area in the dark-field image. Thus, the rhombohedral domains act as nucleation sites for the phase transformation under an applied external electrical field, which in turn leads to the high strain recorded in this material (Zhang *et al.*, 2007; Zhang, Kounga, Aulbach, Granzow *et al.*, 2008).

In the present paper, a ternary system containing BNT, which is solely rhombohedral, BT, consisting of a tetragonal structure, and orthorhombic KNN has been studied. Regarding this mixture of four different *A*-site cations and two different *B*-site cations, a local accumulation of specific cations could lead to a stabilization of one of the three different structures. Likewise, Dorcet & Trolliard (2008) reported the stabilization of the tetragonal structure, induced by the presence of $K^+$ and $Ba^{2+}$ ions. Comparing the samples studied, specimen 92-06-02, with a higher proportion of $K^+$ and $Ba^{2+}$, shows a higher fraction of the tetragonal phase, whereas in sample 94-05-01 the rhombohedral phase is predominant. The possible existence of a monoclinic phase, as often predicted for ferroelectric systems at the MPB, cannot be discarded with the diffraction techniques used here. A possible approach to solving this question could be the application of convergent beam electron diffraction (CBED), comparable to studies of $Pb(Zr_{0.54}Ti_{0.46})O_3$ carried out by Schierholz *et al.* (2008). Nevertheless, the experimenter has to be aware of the fact that the domain width in specimens 92-06-02 and 94-05-01 is in the range of only a few nanometres. Consequently, CBED analysis including several domains would unavoidably lead to symmetry reduction within the CBED pattern, even without the true existence of a monoclinic phase.

## 4. Conclusions

At first glance, the results from powder diffraction and TEM studies seem contradictory, because both types of superlattice reflections are visible in TEM, while neutron diffraction exhibits only one type clearly at a time and X-ray diffraction does not show any superlattice reflections. This discrepancy results from the different length scales and atomic form factors or scattering lengths of the individual experiments. While TEM probes on the local scale of a nanometre-sized sample,

neutron diffraction probes samples of the order of several millimetres.

In sample 92-06-02, the dominant phase is *P*4*bm* and small incorporations of *R*3*c* are visible. Thus, the $a^-a^-a^-$ tilting is not observed, owing to broadening of the selected superlattice reflections, and the absence of reflection splitting in the neutron diffraction data indicates a rhombohedral phase. In specimen 94-05-01, *R*3*c* is the dominant phase. The generally short-range $a^0a^0c^+$ tilting is restricted to even smaller regions, resulting in broadening of the superlattice reflections, which is consistent with the streaking of the 1/2{*ooe*} superstructure reflections in the $[013]_c$ and $[031]_c$ zone axes observed by TEM.

Analysis of the lattice parameters and atomic positions from powder diffraction revealed the nonpolar nature of the *P*4*bm* phase. The antiparallel atomic displacements result in a near extinction of the dipole moment. Together with the pseudocubic lattice, this phase can be characterized as being nonpolar. The *R*3*c* phase in 94-05-01 exhibits a ferroelectric character, with a spontaneous polarization of about 33 $\mu C\,cm^{-2}$. The results indicate a composition-dependent phase transition from a nonpolar to a ferroelectrically active phase, which is in good agreement with the observations of Jo *et al.* (2009).

In this study, a combination of several diffraction techniques, namely X-ray, neutron and electron diffraction, has provided a first insight into the material structure. Understanding the morphology and structure of this new generation of lead-free piezoceramics allows the tuning of the desired material properties for enhanced applications.

This work was funded by the Deutsche Forschungsgemeinschaft, Sonderforschungsbereich 595, Fatigue in Functional Materials. Special thanks are extended to Wook Jo for providing the samples. The authors thank Lars Riekehr for TEM sample preparation and Gerhard Miehe for providing the *PIEP* program. Helpful discussions with Jens Kling, Ian Reaney and George Rossetti Jr are gratefully acknowleged.

## References

Cao, W. & Randall, C. A. (1996). *J. Phys. Chem. Solids*, **57**, 1499–1505.
Dai, X., Xu, Z., Li, J.-F. & Viehland, D. (1995*a*). *J. Mater. Res.* **11**, 618–625.
Dai, X., Xu, Z., Li, J.-F. & Viehland, D. (1995*b*). *J. Mater. Res.* **11**, 626–638.
Dorcet, V. & Trolliard, G. (2008). *Acta Mater.* **56**, 1753–1761.
Frantti, J., Ivanov, S., Eriksson, S., Rundloef, H., Lantto, V., Lappalainen, J. & Kakihana, M. (2002). *Phys. Rev. B*, **66**, 064108.
Glazer, A. M. (1975). *Acta Cryst.* A**31**, 756–762.
Gupta, S. M., Li, J.-F. & Viehland, D. (1998). *J. Am. Ceram. Soc.* **81**, 557–564.
Hoelzel, M., Senyshyn, A., Gilles, R., Boysen, H. & Fuess, H. (2007). *Neutron News*, **18**(4), 23–26.
Jo, W., Granzow, T., Aulbach, E. & Rödel, J. (2009). *J. Appl. Phys.* **105**, 094102.
Jones, G. O. & Thomas, P. A. (2000). *Acta Cryst.* B**56**, 426–430.
Jones, G. O. & Thomas, P. A. (2002). *Acta Cryst.* B**58**, 168–178.
Kishida, K., Goto, K. & Inui, H. (2009). *Acta Cryst.* B**65**, 405–415.
Kling, J. (2010). Personal communication.
Kling, J., Tan, X., Kleebe, H.-J. & Fuess, H. (2010). *J. Am. Ceram. Soc.* In the press.
Maeder, M. D., Damjanovic, D. & Setter, N. J. (2004). *J. Electroceram.* **13**, 385–392.
Miehe, G. (2002). *Program for Interpreting Electron Diffraction Patterns* (*PIEP*). Version 7.12. Institute for Materials Science, Darmstadt University of Technology, Germany.
Rödel, J., Jo, W., Seifert, K. T. P., Anton, E.-M. & Granzow, T. (2009). *J. Am. Ceram. Soc.* **92**, 1153–1177.
Roisnel, T. & Rodriguez-Carvajal, J. (2001). *Mater. Sci. Forum*, **118**, 378381.
Rossetti, G. A. Jr & Khachaturyan, A. G. (2007). *Appl. Phys. Lett.* **91**, 072909.
Saito, Y., Takao, H., Tani, T., Nonoyama, T., Takatori, K., Homma, T., Nagaya, T. & Nakamura, M. (2004). *Nature* (*London*), **84**, 84–87.
Schierholz, R., Fuess, H., Tsuda, K., Ogata, Y., Terauchi, M. & Theissmann, R. (2008). *Phys. Rev. B*, **78**, 024118.
Schmitt, L. A. & Kleebe, H.-J. (2010). *Funct. Mater. Lett.* **3**, 55–58.
Schmitt, L. A., Schönau, K. A., Theissmann, R., Fuess, H., Kungl, H. & Hoffmann, M. J. (2007). *J. Appl. Phys.* **101**, 074107.
Schönau, K. A., Schmitt, L. A., Theissmann, R., Knapp, M., Fuess, H., Eichel, R.-A., Kungl, H. & Hoffmann, M. J. (2007). *Phys. Rev. B*, **75**, 184117.
Takenaka, T., Nagata, H., Hiruma, Y., Yoshii, Y. & Matumoto, K. (2007). *J. Electroceram.* **19**, 259–265.
Tan, X., Aulbach, E., Jo, W., Granzow, T., Kling, J., Marsilius, M., Kleebe, H.-J. & Rödel, J. (2009). *J. Appl. Phys.* **106**, 044107.
Thompson, P., Cox, D. E. & Hastings, J. B. (1987). *J. Appl. Cryst.* **20**, 79–83.
Woodward, D. I., Knudsen I. & Reaney, I. M. (2005). *Phys. Rev. B*, **72**, 104110.
Woodward, D. I. & Reaney, I. M. (2005). *Acta Cryst.* B**61**, 387–399.
Zhang, S.-T., Kounga, A. B., Aulbach, E., Ehrenberg, H. & Rödel, J. (2007). *Appl. Phys. Lett.* **91**, 112906.
Zhang, S.-T., Kounga, A. B., Aulbach, E., Granzow, T., Jo, W., Kleebe, H.-J. & Rödel, J. (2008). *J. Appl. Phys.* **103**, 034107.
Zhang, S.-T., Kounga, A. B., Aulbach, E., Jo, W., Granzow, T., Ehrenberg, H. & Rödel, J. (2008). *J. Appl. Phys.* **103**, 034108.
Zhang, S., Xia, R. & Shrout, T. R. (2007). *J. Electroceram.* **19**, 251–257.